Theoretical Analysis of Oxygen Adsorption on Pt-Based Clusters Alloyed with Co, Ni, or Cr Embedded in a Pt Matrix

P. B. Balbuena,*,† D. Altomare,† L. Agapito,‡ and J. M. Seminario*,‡

Department of Chemical Engineering and Department of Electrical Engineering, University of South Carolina, Columbia, South Carolina 29208

Received: June 18, 2003; In Final Form: August 4, 2003

A systematic evaluation of the oxygen molecule dissociation on metal and metal alloy surfaces is performed to determine optimal catalytic materials for oxygen dissociation. The study focuses on the physical, chemical, and electrical characteristics at the oxygen−metal interface where the effects of the oxygen molecule and the metal atoms in its neighborhood, as well as the effects of the extended and continuum nature of the catalyst, are considered through the use of molecular and extended ab initio procedures interconnected by a Green function formalism to account for the interfacial characteristics.

1. Introduction

Chemisorption of molecular oxygen takes place on platinum surfaces via an initial adsorption state in which partial charge transfer precedes oxygen dissociation.[1−4] Oxygen is also reduced electrochemically, where a first one-electron reduction is considered the rate-determining step in the four-electron reduction of oxygen in acid medium, yielding water as the final product.[1,5−7] The overall reduction reaction is

$$O_2 + 4e^- + 4H^+ \xrightarrow{\text{catalyst}} 2H_2O$$

and proposed first one-electron equations are

$$O_2 + e^- \xrightarrow{\text{catalyst}} (O_2^-)_{\text{adsorbed}}$$

or a coupled electron and proton transfer

$$O_2 + e^- + H^+ \xrightarrow{\text{catalyst}} (O{-}OH)_{\text{adsorbed}}$$

Platinum electrodes are used as electrocatalysts of the oxygen reduction, and so far, platinum is the preferred cathode material for low-temperature fuel cells.[7] Under the actual assembly conditions, such electrocatalysts can be defined as complex composite materials, where nanoparticles of the active catalyst are usually dispersed on a carbon support and embedded in a polymer electrolyte, which is the medium in which protons travel to the surface of the catalyst.[8,9] Air diffuses through that medium, and oxygen is reduced at the metal surface. Because of the high cost of platinum and the slow kinetics of the oxygen reduction, major research efforts tend to find alternative catalysts.[10,11] Recent experiments[10,12−14] indicated that effective alloys made with Pt−Co, Pt−Cr, and Pt−Ni are at least as good as pure Pt, and in many cases, the alloyed material showed a better performance for the O_2 electroreduction; however, the reasons for such behavior are still unknown.

The present work is an attempt to determine the factors for the effectiveness of specific alloys toward the oxygen dissociation and reduction, using a systematic methodology to investigate the physical, chemical, and thermodynamic behavior of Pt−M alloy clusters and their interactions with the bulk material for the adsorption and dissociation of molecular oxygen.

2. Theoretical Methods

Our approach consists of finding physical, chemical, and electrical characteristics at reaction sites that are due to interactions of the reactant molecule and the metal atoms in its neighborhood, as well as to the effect of the continuum nature of the catalyst. The discrete and continuum information are put together through a Green function approach developed for the study of nanoscopic junctions in molecular electronics. We briefly describe these procedures.

Finite Systems. The Becke-3 Perdew−Wang 91 (B3PW91)[15−17] hybrid functional is used in combination with LANL2DZ pseudopotential and basis set[18−20] as implemented in the Gaussian 98 program.[21] This combination is the most effective level of theory available for the analysis of metallic systems; several applications have been already reported.[17] B3PW91 is a fully nonlocal functional consisting of the generalized gradient approximation (GGA) of Becke[15] for the exchange functional mixed with a contribution calculated a la Hartree−Fock. The correlation contribution is calculated using the ab initio GGA PW91[16,17] correlation functional. The B3PW91 when used with the LANL2DZ[18−20,22] basis set (B3PW91/LANL2DZ) provides excellent results when metallic atoms are used.[23−26] In these calculations, we have used the 6-31G basis set for the oxygen atoms; this is referred to as the B3PW91/LANL2DZ/O:6-31G level of theory. All systems were fully optimized at this level of theory. Once forces are zeroed, a second derivative calculation is performed to ensure that a minimum in the potential energy surface is reached; thus, only minimum energy configurations are used in these calculations. A second derivative of the energy calculation is also performed for all systems to determine stability and zero-point energies. Atomic charges are estimated using Mulliken population analysis,[27] which associates charges to each atom by integrating the density contribution of the basis functions assigned to each

* Corresponding authors. E-mail addresses: balbuena@engr.sc.edu; jsemina@engr.sc.edu.
† Department of Chemical Engineering.
‡ Department of Electrical Engineering.

10.1021/jp035729j CCC: $25.00
Published on Web 11/15/2003

individual atom and assigning equal overlap contributions to both atoms of every pair. Notice that atomic charges are not expectation values but mere indicators highly dependent on the method and basis set used to solve the Schrödinger equation; these indicators provide qualitative analysis and interpretations of charge-transfer effects, and they are not used to draw conclusions but rather to provide a qualitative picture of the quantitative results. Full description of the DFT methods in Gaussian 98 for the molecular systems can be found elsewhere.[28,29]

Infinite Systems. Crystal 98[30] is used to study the bulk metallic systems with periodic boundary conditions using DFT[31] within the linear combination of atomic orbitals approximation.[32] The basis expands the Bloch functions built using *s*, *p*, and *d* Gaussian functions:

$$\Psi_k(r+g) = \Psi_k(r)\exp(ikg) \tag{1}$$

and the electron density of the *N*-electron system[31] is given by

$$\rho(r) = \int_{\substack{\text{Brillouin}\\ \text{zone}}} \mathrm{d}k \sum_{i}^{\substack{\text{occupied}\\ \text{bands}}} |\varphi_{ki}(r)|^2 \theta(\epsilon_F - \epsilon_i(k)) \tag{2}$$

where θ is the Heaviside step function, $\epsilon_i(k)$ is the eigenvalue of the *i*th crystalline orbital, and ϵ_F is the Fermi energy. The Bloch functions described above are used to expand the crystalline orbitals that are linear combinations of atom-centered Gaussian-type functions, $\varphi_{ki}(r)$. The coefficients for the linear expansion are adjusted so that $\varphi_{ki}(r)$ are the solutions of the one-particle equations:

$$\hat{h}_i\varphi_{ki}(r) = \epsilon_{ki}\varphi_{ki}(r) \tag{3}$$

where $\hat{h}$ is the single-particle Hamiltonian operator,

$$\hat{h}_{KS} = \hat{t} + \hat{v} + J[\rho(r)] + \hat{v}_{xc}(r) \tag{4}$$

which includes the contributions from kinetic, external potential, Coulomb, and exchange−correlation potential operators, respectively. The exchange−correlation operator is expanded in a basis of Gaussian-type functions.

$$v_{xc}^{i,jg} = \int \mathrm{d}r\, \chi_i(r - s_i) v_{xc}(r) \chi_i(r - s_j - g) \tag{5}$$

g is the cell containing the *j*th basis function centered at the atomic position s_j. This integral is solved analytically because the exchange−correlation potential is expanded with Gaussian auxiliary basis functions, $G_a(r)$; thus, the integral is transformed into a linear combination of integrals of the form

$$g_a^{i,jg} = \int \mathrm{d}r\, \chi_i(r) G_a(r) \chi_i(r - s - g) \tag{6}$$

which are solved only once and then stored for subsequent use. At each step, the coefficients are recalculated so that the exchange−correlation potential fits the analytic form that depends on the charge density. We use the hybrid functional approach with the gradient-corrected PW91 functionals[16] for the correlation potential, together with the SBKJC VDZ ECP (8s8p6d)/(4s4p3d) basis sets.[33,34] The Pt bulk is treated as an infinite periodic system with fcc crystalline structure; thus, realistic density of states for metals is obtained to construct the Green function for the catalyst. In turn, we can also determine the parameters for a catalyst with an arbitrary shape simply by providing a suitable geometry obtained with the program Gaussian 98.

Green Function Approach. Effects on single molecules attached to a bulk metal are obtained using our combined DFT−Green function technique.[25,35] This method, originally developed to provide transport properties of electrons going through molecular systems, combines information obtained for contacts or reservoirs (in this case, the catalyst surface) by an ab initio procedure for extended systems and that for the molecule (the adsorbate) calculated by an ab initio procedure for single molecules. Notice that in a real system molecules are chemically attached to real catalysts, made of atoms, and not to ideal surfaces. Therefore, information about the interface is provided through coupling matrices obtained at a molecular level using the information from the extended molecule (i.e., the molecule attached to a few atoms from the catalysts) provided by Gaussian 98. Thus, our calculations consider explicitly the chemistry of the attachment of the molecule to the catalyst instead of unrealistic simulations of a molecule attached to a perfect or ideal surface.

The Hamiltonian of the extended molecule, written in atomic orbitals (AO) bases, is partitioned into submatrices for the isolated molecule (H_{MM}) and the couplings between the molecule (subscript M) and the atoms of the catalyst (subscripts 1 and 2 for a two-point attachment).

$$H_{KS} = \begin{bmatrix} H_{11} & H_{1M} & H_{12} \\ H_{M1} & H_{MM} & H_{M2} \\ H_{21} & H_{2M} & H_{22} \end{bmatrix} \tag{7}$$

This Hamiltonian for the extended molecule can also be recalculated in case of an external field to account for the reorganization of the molecular electronic structure due to the presence of such field, including among others, the effects of charge transfer between the molecule and the catalyst. Notice that the molecule itself does not have an integer charge for any of the charge states of the extended molecule because the charge distributes between the isolated molecule and the metal atoms. Charge transfers between molecule and catalyst occur even at zero bias and also as a result of externally applied fields. Certainly, this charge transfer is limited because of the small number of metal atoms attached to the molecule, which is not a major problem because it is clearly demonstrated from theoretical as well as experimental information[36−38] that the connection of the molecule to the metal is only through one or two metal atoms as concluded in ref 36; however, the interactions with the atoms located beyond these nearest neighbors are very small and truncated. This constitutes the major weakness of our procedure. Fortunately, there is strong evidence that it is an acceptable approximation because it precisely considers the chemistry and physics of the actual local attachment or bonding of the molecule to the catalyst atoms.[37,39]

The coupling between atoms of the catalyst and those of the molecule yields the complex interaction terms, Σ_i, which account for the broadening of the molecular electronic levels and depend on the complex Green function, g_i, describing the catalysts

$$\Sigma_i = H_{Mi} g_i H_{iM} \tag{8}$$

The density of states (DOS) and its *s*, *p*, and *d* contributions as a function of the energy are obtained for platinum (or any other) crystal from its optimized geometry and its converged electronic

structure. Thus, the Green function for the metallic catalyst (g_i) is given by

$$g_i(E) = \pi i \times \begin{bmatrix} g_i^1 & \cdots & 0 \\ \vdots & \ddots & \vdots \\ 0 & \cdots & g_i^{n_i} \end{bmatrix} \tag{9}$$

with

$$g_i^k(E) = \begin{bmatrix} D_i s^k(E) & 0 & 0 & 0 \\ 0 & D_i p^k(E) & 0 & 0 \\ 0 & 0 & D_i d_{t_2 e}^k(E) & 0 \\ 0 & 0 & 0 & D_i d_{e_g}^k(E) \end{bmatrix} \tag{10}$$

The index k runs over the atoms representing the catalyst such that the size of the g_i matrix is equal to the number of columns (rows) in the coupling matrix H_{Mi} (H_{iM}). The complex g_i can be obtained from any source as long as it can be represented in matrix form of appropriate dimensions; it provides the information from the catalyst to the DFT−GF formalism. We choose to generate the Green function for the catalyst using Crystal 98 because it allows us to obtain a high-level electronic structure of a bulk system of any shape using DFT; however, the coupling to the molecule is obtained from molecular calculations (H_{iM} and H_{Mi} in the extended molecule Hamiltonian, shown in eq 7) that consider the atomistic nature of the catalyst−molecule interface. The interaction terms defined in eq 8 are added to the molecular Hamiltonian to account for the effect of the catalyst on the molecule:

$$H_e = \begin{bmatrix} H_{11} & H_{1M} & H_{12} \\ H_{M1} & H_{MM} + \Sigma_1 + \Sigma_2 & H_{M2} \\ H_{21} & H_{2M} & H_{22} \end{bmatrix} \tag{11}$$

To account for the nonorthogonality of the basis set, the overlap matrix modifies the Hamiltonian into

$$H'_e = S^{-1} H_e \tag{12}$$

And the corresponding H_{MM}

$$H_{MM} = H'_{MM} + \Sigma'_1 + \Sigma'_2 \tag{13}$$

yields the Green function for a molecule attached to two atoms of the catalyst,

$$G_M = [EI - H'_{MM}]^{-1} \tag{14}$$

The density of states (DOS) is obtained from the Green function according to

$$\mathrm{DOS} = \mathrm{tr}[i(G_M - G_M^+)] \tag{15}$$

Within the Green function formalism, two separated and independent calculations are needed, a molecular calculation on the molecule of interest plus a few atoms such as those in the catalyst and a calculation of the density of states of the catalyst. Those calculations can be performed at any level of theory; however, it is desirable to choose ab initio methods known to provide acceptable chemical accuracy, such as DFT using generalized gradient approximation or better.

TABLE 1: Energies and Multiplicities ($m = 2S + 1$) at the B3PW91/LANL2DZ/O:6-31G Level of Ground States of All Systems Treated in This Work

system	energy (hartree)	m	ZPE (hartree)
O_2	−150.21010	3	0.00334
Cr_2	−172.53896	5	0.00036
Co_2	−290.15449	5	0.00057
Ni_2	−338.59411	5	0.00056
Pt_2	−238.31634	3	0.00043
PtCr	−205.50418	5	0.00047
PtCo	−264.23249	4	0.00068
PtNi	−288.48659	3	0.00054
Pt_3	−357.56051	1	0.00125
$CrPt_2$	−324.73578	5	0.00136
$CoPt_2$	−383.49353	4	0.00150
$NiPt_2$	−407.71474	3	0.00133
$PtCr_2$	−291.83976	3	0.00095
$PtCo_2$	−409.38512	5	0.00137
$PtNi_2$	−457.85607	3	0.00144
O_2Pt_2	−388.57852	1	0.00577
O_2PtCo	−414.52314	4	0.00635
O_2PtCr	−355.77616	5	0.00575
O_2PtNi	−438.75284	3	0.00590
O_2Co_2	−440.42886	7	0.00543
O_2Cr_2	−322.94292	11	0.00478
O_2Ni_2	−488.88834	5	0.00605
O_2Pt_3	−507.81033	3	0.00642
$O_2PtPtCo$	−533.72638	4	0.00646
$O_2PtPtCr$	−474.95981	5	0.00634
$O_2PtPtNi$	−557.95883	3	0.00642
$O_2CoPtPt$	−533.75879	6	0.00646
$O_2CrPtPt$	−475.00378	7	0.00634
$O_2NiPtPt$	−557.98181	5	0.00642
$O_2PtCoCo$	−559.64817	7	0.00627
$O_2PtCrCr$	−442.09582	5	0.00629
$O_2PtNiNi$	−608.11333	3	0.00636
$O_2CoCoPt$	−559.70288	7	0.00683
$O_2CrCrPt$	−442.16323	3	0.00590
$O_2NiNiPt$	−608.14473	5	0.00681

3. Results and Discussion

Analysis of Metal and Oxygenated Clusters. The B3PW91/LANL2DZ/O:6-31G total energies and zero-point energies for the lowest-energy (ground-state) structures of all systems analyzed in this work are listed in Table 1, along with the corresponding multiplicity, $m = 2S + 1$, for the spin (S) of each ground state. All clusters are fully optimized, and second-derivative calculations at their optimized geometries show that all systems correspond to local minima, that is, there are no imaginary frequencies. As expected, dimers and trimers involving Pt, Cr, Co, and Ni, as well as their complexes with adsorbed oxygen exhibit high multiplicities in their ground state, except for Pt_3, which is a singlet in its ground state; however, a triplet state is just 0.01 eV higher (vide infra).

It is important to mention that the calculation of transition metal dimers is very difficult and predictions of their energies are a challenge to the most sophisticated ab initio procedures. At this point, there is not way to predict the correct multiplicity of dimers using any method, and in particular, the practical methods such as DFT offer additional problems because the energies reported, do not correspond to real systems but to ideal systems of noninteracting electrons. However calculations improve for systems bigger than a dimer because of the mutual contributions of basis sets from a larger number of atoms. Although this brings about other problems, like basis set superposition errors, it helps when the goal is to determine

TABLE 2: Binding Energies of O_2 to a Bridge Site of Metallic Clusters[a]

reaction	product energy (hartree)	reactants energy (hartree)	−binding energy (eV)
$O_2 + Pt_2 \rightarrow O_2Pt_2$	−388.57852	−388.52644	1.42
$O_2 + PtCo \rightarrow O_2PtCo$	−414.52314	−414.44259	2.19
$O_2 + PtCr \rightarrow O_2PtCr$	−355.77616	−355.71428	1.68
$O_2 + PtNi \rightarrow O_2PtNi$	−438.75284	−438.69669	1.53
$O_2 + Co_2 \rightarrow O_2Co_2$	−440.42886	−440.36459	1.75
$O_2 + Cr_2 \rightarrow O_2Cr_2$	−322.94292	−322.74906	5.28
$O_2 + Ni_2 \rightarrow O_2Ni_2$	−488.88834	−488.80421	2.29
$O_2 + Pt_3 \rightarrow O_2Pt_3$	−507.81033	−507.77061	1.08
$O_2 + Pt_2Co \rightarrow O_2PtPtCo$	−533.72638	−533.70363	0.62
$O_2 + Pt_2Cr \rightarrow O_2PtPtCr$	−474.95981	−474.94588	0.38
$O_2 + Pt_2Ni \rightarrow O_2PtPtNi$	−557.95883	−557.92484	0.92
$O_2 + Pt_2Co \rightarrow O_2PtCoPt$	−533.75879	−533.70363	1.50
$O_2 + Pt_2Cr \rightarrow O_2PtCrPt$	−475.00378	−474.94588	1.58
$O_2 + Pt_2Ni \rightarrow O_2PtNiPt$	−557.98181	−557.92484	1.55
$O_2 + Co_2Pt \rightarrow O_2PtCoCo$	−559.64817	−559.59522	1.44
$O_2 + Cr_2Pt \rightarrow O_2PtCrCr$	−442.09582	−442.04986	1.25
$O_2 + Ni_2Pt \rightarrow O_2PtNiNi$	−608.11333	−608.06617	1.28
$O_2 + Co_2Pt \rightarrow O_2CoCoPt$	−559.70288	−559.59522	2.93
$O_2 + Cr_2Pt \rightarrow O_2CrCrPt$	−442.16323	−442.04986	3.09
$O_2 + Ni_2Pt \rightarrow O_2NiNiPt$	−608.14473	−608.06617	2.14

[a] In the triatomic metallic clusters O_2XYZ, O_2 is adsorbed on the XY bridge site.

ground states. Thus, because ground states are calculated correctly by DFT, working with the lowest-energy systems provides confidence that results are correct for such states, although the determination of their corresponding multiplicity is not unambiguous because the calculated multiplicity would be that of the noninteracting system used as an auxiliary wave function in DFT.

Numerous studies have indicated that O_2 adsorbs molecularly on Pt surfaces below 150 K,[40] and two precursors for chemisorption have been found:[40,41] a superoxo state, which adsorbs in a tilted bridge site (at distances between 1.9 and 2 Å from the surface), and a peroxo state in which O_2 is adsorbed in a parallel bridge site at about 1.8 Å from the surface. These states have been identified theoretically on clusters[42,43] and in extended surfaces.[44,45] For this reason, we have chosen to test the bridge site adsorption of O_2. Table 2 shows the binding energy (BE) of the oxygen molecule adsorbed to the bridge site of several bi- and triatomic metallic clusters. BE is defined as the difference between the product ground-state energy and the sum of the ground-state energies of the reactants. The oxygen molecule adsorbed on a bridged site of a metallic trimer yields a system referred to as O_2PtPtX if O_2 adsorbs on the Pt−Pt bond, O_2XPtPt if O_2 adsorbs on the X−Pt bond, and O_2XXPt if O_2 adsorbs on the X−X bond. O_2 adsorbs to a Pt−Pt bridge site (in Pt_2) releasing 1.42 eV, and that energy is 0.77 eV higher when one of the Pt atoms is substituted by Co, 0.26 eV higher for PtCr, and 0.11 eV higher for PtNi (Table 2). If both Pt atoms in O_2Pt_2 are substituted by Co, Cr, or Ni, the O_2 binding energies are also significantly enhanced, especially in the case of O_2Cr_2, for which the calculated release of energy is 5.28 eV; this effect is due to Cr oxidation as discussed below in relation to Table 4. The presence of a third Pt atom decreases the O_2Pt_2 binding energy by 0.34 eV. Substitution of that third Pt atom by Ni (yielding $O_2PtPtNi$) causes the BE relative to $O_2PtPtPt$ to be reduced only by 0.16 eV; however, if the third atom is Co or Cr, the BE decreases are 0.46 and 0.7 eV, respectively.

Comparing the values of the BEs corresponding to trimers O_2PtXPt, in which O_2 adsorbs on the PtX bridge site, to those in the O_2PtX complexes, we observed that the presence of the second Pt atom reduces the O_2 BE in $O_2PtCoPt$ by 0.69 eV, but less dramatic effects are found in $O_2PtCrPt$ for which there is a small decrease of 0.10 eV, whereas the effect is negligible (an increase of only 0.02 eV) in $O_2PtNiPt$. Although their O_2 BEs are reduced (or very slightly increased) with respect to O_2PtX, the three O_2PtXPt complexes exhibit enhanced BEs with respect to $O_2PtPtPt$. Similarly, when a second X atom is added to the O_2PtX system, yielding O_2PtXX, the BEs are further reduced with respect to those in O_2PtXPt, but still all of them are enhanced compared to the BE of O_2 to Pt_3.

The binding energies of the last group of compounds in Table 2, O_2XXPt, illustrate that the effect of the Pt atom on the BE (compared to those in O_2XX) is negligible for Ni, but opposite effects are seen in $O_2CoCoPt$ for which the BE is 1.18 eV higher than that in O_2CoCo, whereas in $O_2CrCrPt$, the BE is reduced by 2.19 eV with respect to O_2CrCr. The BEs of the three O_2XXPt compounds are, however, enhanced with respect to that of $O_2PtPtPt$. In summary, the presence of Co, Cr, and Ni as one or two of the elements in the bridge site where O_2 adsorbs results in an enhancement of the binding energy of O_2 to the cluster compared to the cases of pure Pt clusters. The most exothermic adsorptions are found when O_2 adsorbs to the XX bridge site, and an opposite effect (decrease of the binding energy) is observed in the O_2PtPtX clusters (X is Co, Cr, or Ni). Further discussion and interpretation of these behaviors is given below (see also Tables 4 and 5) in relation to the geometric and electronic changes observed in the clusters upon O_2 adsorption.

Several spin states were analyzed to determine the lowest state for every one of the chosen systems. The results are shown in Table 3. Spin states with less than 1 eV energy separation from the ground state are reported, implying the probability of coexistence of alternative states, in some cases of higher reactivity due to the presence of a large number of unpaired electrons, such as the CrCr ($m = 7$) state, 0.13 eV higher than the ground-state quintet, and $O_2PtPtCr$ for which the $m = 7$ state is only 0.01 eV higher in energy than the ground-state quintet. Co compounds also exhibit similar behavior, for example, in $O_2CoCoPt$ for which the $m = 5$ state is 0.02 eV higher in energy than the ground-state septet.

In all cases, adding at least one X atom (X = Co, Cr) to Pt or Pt_2, increases the ground-state multiplicity, as expected on the basis of the electronic structures of these elements. Thus, the calculated most-stable states of PtCr, PtCrCr, and Pt_2Cr are quintet states, whereas quartets are found in the corresponding Co compounds and triplets when X = Ni (Table 1), which gives a preliminary indication about higher reactivity expected in the Cr and Co compounds as compared with Ni. Such property is enhanced upon O_2 adsorption, where the XX dimers of Cr and Co also exhibit very high multiplicity in their ground states, in particular, O_2CoCo ($m = 7$) and O_2CrCr ($m = 11$). When a Pt atom is added, the multiplicity of O_2CoCo remains as 7, whereas that of $O_2CrCrPt$ reduces to 3, which may be associated with changes in the oxidation states in the Cr atoms.

Although the electronic structures of Pt($[Xe]4f^{14}5d^{9}6s$) and Ni($[Ar]3d^{8}4s^{2}$) are more alike than those of Pt compared to Co-($[Ar]3d^{7}4s^{2}$) and Pt compared to Cr ($[Ar]3d^{5}4s$), the presence of Ni also increases the spin state of NiPt dimers or trimers complexed with O_2. Thus, it can be concluded that Ni, Co, and Cr make Pt-based complexes more "reactive" because they enable a higher number of unpaired electrons.

Table 4 contains four sets of data: The first group (first five rows) corresponds to O_2 adsorption on the Pt−Pt bridge site. The second group corresponds to O_2 adsorption on the Pt−X bond (X = Cr, Co, Ni) of PtXPt. The third group corresponds

TABLE 3: Energy Differences (in eV) between the Ground State and Higher Energy States for Systems in Table 1

molecule	$m = 1$	$m = 2$	$m = 3$	$m = 4$	$m = 5$	$m = 6$	$m = 7$	$m = 8$	$m = 9$	$m = 11$	$m = 13$
					X_1X_2						
CoCo	4.37		0.80		0.00		0.57				
CrCr	2.12		2.05		0.00		0.13				
NiNi	1.08		0.44		0.00		3.09				
PtPt	1.62		0.00		0.89						
PtCr	5.44		2.95		0.00		0.34		1.98		
PtNi	0.79		0.00		1.31		3.69		10.11		
PtCo		0.64		0.00		1.04					
					$O_2X_1X_2$						
O_2CoCo	2.84		0.72		0.46		0.00		1.25		
O_2CrCr	5.80		3.81		2.31		2.08		0.92	0.00	1.62
O_2NiNi	3.61		0.24		0.00		1.37				
O_2PtPt	0.00		0.70								
O_2PtCr	1.65		0.40		0.00		0.48		1.50		
O_2PtNi	0.11		0.00		0.45		2.16		6.30		
O_2PtCo		0.48		0.00		0.41		2.00			
					PtPtX						
PtPtPt	0.00		0.01		1.09						
PtPtCr	3.34		0.54		0.00		0.46				
PtPtNi	0.59		0.00		0.43						
PtPtCo		0.44		0.00		0.82					
					PtXX						
PtCoCo	3.77		0.75		0.00		0.21				
PtCrCr	4.20		0.00		1.40						
PtNiNi	1.36		0.00		0.43						
					O_2PtPtX or O_2XPtPt						
O_2PtPtCo		0.85		0.00		0.16					
O_2PtPtCr	3.87		0.17		0.00		0.01				
O_2PtPtNi	1.34		0.00		0.33						
O_2PtPtPt	0.50		0.00		0.29						
O_2CoPtPt		0.13		0.11		0.00		1.32			
O_2CrPtPt	2.59		1.16		0.19		0.00		0.80		
O_2NiPtPt	1.03		0.12		0.00		1.39				
					O_2PtXX or O_2-XXPt						
O_2PtCoCo	3.46		0.79		0.02		0.00		0.64		
O_2PtNiNi	1.58		0.00		0.03		0.82				
O_2PtCrCr	2.94		2.64		0.00		0.19				
O_2CrCrPt	1.41		0.00		0.81						
O_2CoCoPt	3.09		1.27		0.43		0.00		1.44		
O_2NiNiPt	1.75		0.19		0.00		1.27				

to O_2 adsorption on the Pt−X bond of PtXX, and the last group corresponds to O_2 adsorption on the X−X bond of XXPt. For comparison purposes, each group includes the properties of O_2 adsorbed on the corresponding dimer. The following conclusions are drawn from Table 4:

(a) In comparison with the properties observed in O_2PtPt and O_2PtPtPt, when a third atom (X) is added to the Pt_2 cluster forming a triangular PtPtX structure, and the *O_2 molecule is adsorbed on the Pt−Pt bridge site*, the O−O bond length of the adsorbed molecule is shorter than that in O_2PtPt (1.54 Å) and O_2PtPtPt (1.41 Å), indicating a lesser degree of O_2 dissociation, the charges on each of the adsorbed O atoms are less negative (Table 4), and the O_2 molecule is located farther from the cluster as indicated by the longer values of the O−Pt distance. Thus, the presence of the X atom does not favor oxygen adsorption on the Pt−Pt bridge site, as reflected also by the decrease of the binding energies of the O_2PtPtX relative to those of O_2PtPtPt. The reason for this behavior is that the X atoms in O_2PtPtX tend to become oxidized at the expense of the Pt atoms that become slightly negatively charged (the highest negative charges in O_2PtPtX are found for X = Cr), whereas the charge-transfer (reduction) effect of the Pt atoms on the oxygen atoms is less effective than that in O_2Pt_3.

(b) When the *O_2 molecule is adsorbed on the Pt−X bridge site* of PtXPt, in comparison with the O_2PtPtPt adsorption, the O−O bond elongates (by 0.06 Å) for X = Cr and for Co (increases by 0.04 Å) and remains about the same (shortened only by 0.01 Å) for X = Ni. Both Mulliken charges on the O atom adsorbed on X and those of the O adsorbed on Pt are more negative than those in O_2Pt_3. The charges on the O atom closest to X are 0.16*e*, 0.12*e*, and 0.06*e* more negative when X = Cr, Co, and Ni, respectively. The O−X and O−Pt distances are shorter than O−Pt in O_2PtPtPt (except for O−Ni, 0.01 Å longer), and O−X is always shorter than O−Pt in the O_2PtXPt complexes. Thus, there is a clear strong interaction between O and X that favors O_2 dissociation; X becomes oxidized, whereas both Pt and O_2 become reduced. As discussed in a previous section, the O_2 binding energies in O_2PtXPt are higher than those in O_2PtPtPt, which is another evidence of enhanced chemisorbed states.

(c) When the *O_2 molecule is adsorbed on the Pt−X bridge site* of PtXX, that is, a case equivalent to that discussed in point b but with an X neighbor instead of a Pt neighbor, the changes are similar but less pronounced than those observed for O_2 adsorbed on the PtX bridge site of PtXPt. The charges on the O atom closest to X are 0.10*e*, 0.08*e*, and 0.05*e* more negative when X = Cr, Co, and Ni, respectively, whereas that on the O atom connected to Pt is 0.04*e* more negative when X = Ni but slightly less negative when X = Cr and Co. In this case, the extra metal atom X that is not directly connected to oxygen atoms becomes also oxidized at the expense of Pt, which is partially reduced, but still is able to reduce O_2 more effectively

TABLE 4: Mulliken Charges (*Q*, in *e*), Distances (*r*, in Å), and Binding Energy (BE, in eV) of O_2 Absorbed on Metallic Clusters[a]

system	Q_{O1}	Q_{O2}	Q_{X1}	Q_{X2}	r_{O1-O2}	r_{O1-X1}	r_{O2-X2}	r_{X1-X2}	−BE
$O_2PtPtPt$	−0.21	−0.21	0.22	0.22	1.41	2.06	2.06	2.41	1.08
O_2PtPt	−0.31	−0.31	0.31	0.31	1.54	1.93	1.93	2.53	1.42
$O_2PtPtCo$	−0.19	−0.19	−0.06	−0.06	1.38	2.10	2.10	2.43	0.62
$O_2PtPtNi$	−0.19	−0.19	−0.06	−0.06	1.38	2.09	2.09	2.43	0.92
$O_2PtPtCr$	−0.21	−0.18	−0.11	−0.14	1.37	2.06	2.15	2.48	0.38
$O_2PtCoPt$	−0.26	−0.33	0.04	0.81	1.45	2.01	1.90	2.52	1.50
O_2PtCo	−0.29	−0.34	−0.13	0.76	1.50	1.95	1.82	2.40	2.19
$O_2PtNiPt$	−0.20	−0.27	−0.02	0.74	1.40	2.07	1.95	2.47	1.55
O_2PtNi	−0.26	−0.28	−0.10	0.63	1.44	1.93	1.86	2.44	2.87
$O_2PtCrPt$	−0.29	−0.37	−0.02	0.96	1.47	1.99	1.90	2.52	1.56
O_2PtCr	−0.31	−0.40	−0.17	0.88	1.52	1.96	1.83	2.48	1.68
$O_2PtCoCo$	−0.20	−0.29	−0.21	0.42	1.40	2.10	2.02	2.38	1.44
$O_2PtNiNi$	−0.25	−0.26	−0.19	0.41	1.41	2.06	1.87	2.44	1.28
$O_2PtCrCr$	−0.17	−0.31	−0.45	0.51	1.41	2.15	1.89	2.56	1.25
$O_2CoCoPt$	−0.38	−0.38	0.63	0.63	1.49	1.82	1.82	2.63	2.93
O_2CoCo	−0.37	−0.37	0.37	0.37	1.51	1.85	1.85	2.37	1.75
$O_2NiNiPt$	−0.24	−0.24	0.45	0.45	1.38	1.98	1.98	2.34	2.14
O_2NiNi	−0.34	−0.34	0.34	0.34	1.48	1.83	1.83	2.32	2.29
$O_2CrCrPt$	−0.33	−0.30	0.67	0.56	1.41	1.81	2.12	2.72	3.09
O_2CrCr	−0.40	−0.40	0.40	0.40	1.51	1.87	1.87	2.71	5.28

[a] The two atoms closest to the oxygen atoms O1 and O2 are named X1 and X2, respectively. The first five rows correspond to O_2 adsorption on the Pt−Pt bridge site. In the next six rows, O_2 adsorbs on the Pt−X bond (X is Cr, Co, or Ni) of PtXPt. The following three rows correspond to O_2 adsorbing on the Pt−X bond of PtXX, and the last six rows display results of O_2 adsorption on the X−X bond of XXPt. For comparison, each group includes the properties of O_2 adsorbed on the corresponding dimer. X_1 and X_2 are the atoms of the bridge site where O_2 is adsorbed.

than in the case of $O_2PtPtPt$. On the other hand, the X atom connected to O_2 is oxidized but to a lesser degree, causing the O_2 reduction to be a little less effective than that in O_2PtXPt. The O−O distances in the adsorbed state of O_2PtXX are identical to that in $O_2PtPtPt$, except when X = Co, for which the O−O distance is 0.01 Å shorter. The distance between X and the closest O atom is in all cases shorter than the O−Pt distance in $O_2PtPtPt$; however, these distances are slightly elongated with respect to those in O_2PtXPt (Table 4). The binding energies are higher than those in $O_2PtPtPt$.

(d) When the *O_2 molecule is adsorbed on the X−X bridge site* of PtXX, the induced changes relative to O_2Pt_3 depend on X. The metal that most favors O_2 dissociation on the X−X bridge site is Co, followed by Cr, and finally Ni. This order may be associated with the easiness of these elements to switch to high oxidation states. There is charge transfer due to X oxidation from the X atoms to the rest of the system, especially in the cases of X = Co and Cr, which is evidenced by the high negative charges on the two adsorbed oxygen atoms. The adsorption mode is parallel to the XX bond, except in the case of $O_2CrCrPt$ where a tilted mode is favored (Table 4), which results in the strongest binding energy (−3.09 eV), almost three times larger than that in $O_2PtCrCr$. However, the O−O bond length (1.41 Å) does not show further dissociation than in the case of $O_2PtPtPt$, indicating that despite the strong chemisorption the CrCr bond would be as good as but not better than a PtPt bond, whereas the PtCr bond that induces a separation O−O of 1.47 Å, along with a binding energy of −1.56 eV, may be a better contributor to O_2 dissociation in Pt−Cr alloys. The case of $O_2CoCoPt$ is the best of this group from the point of view of favoring O_2 dissociation. The O−O separation in this complex (1.49 Å) is the largest in all of the O_2−trimer complexes in this study, and also the largest negative charges are those on each of the O atoms attached to the Co−Co bond (−0.38*e*), whereas the O−X distances are the shortest (1.82 Å). It is also interesting that this is the only case for which the presence of

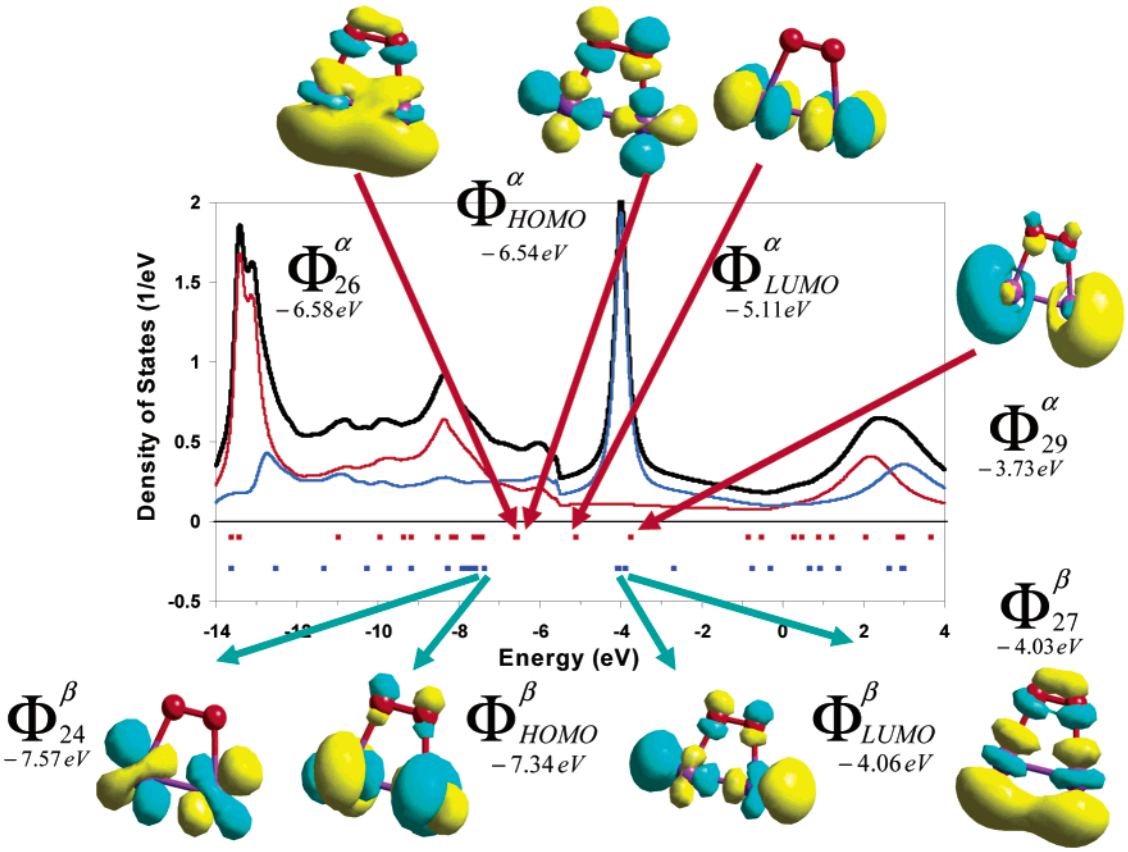

Figure 1. Density of states of the oxygen molecule chemisorbed to Pt_2. A background of Pt states is added through the Green function methodology. The Fermi level of Pt is located at −5.93 eV. The red and blue symbols are the energies of the discrete molecular orbitals of O_2Pt_2.

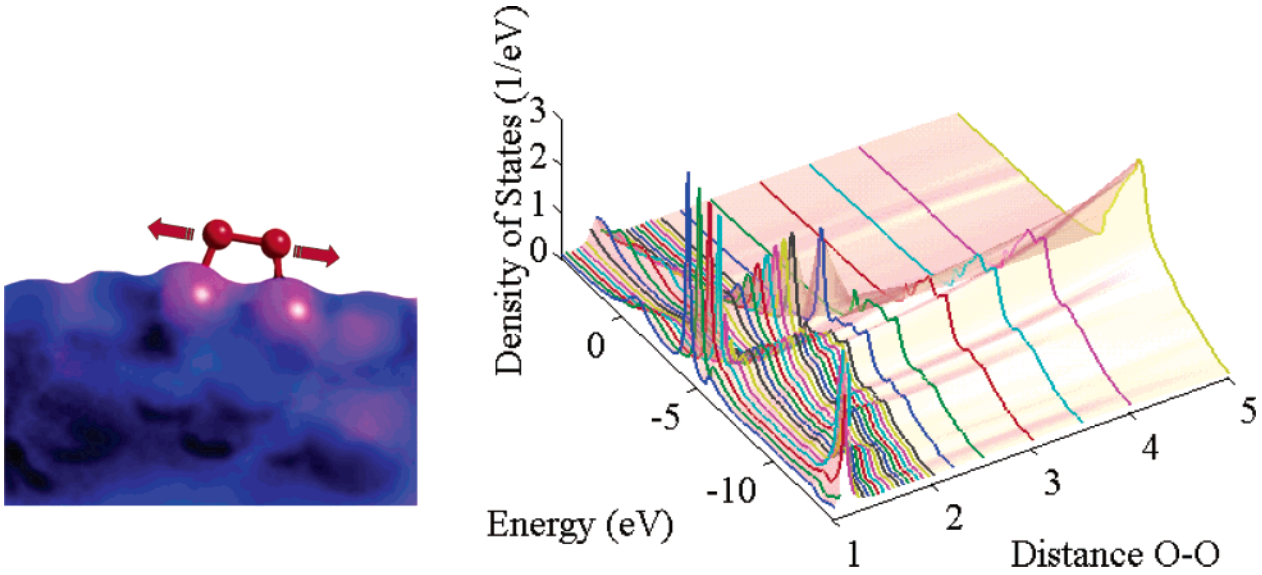

Figure 2. The center of the O−O bond is located at 2.10 Å from the center of the Pt−Pt bond. The Pt−Pt (2.47 Å) and the Pt−O bond distances are kept constant, whereas the O−O bond length is varied progressively from the gas-phase O−O bond length, 1.2 Å, to 5 Å under the influence of a Pt background.

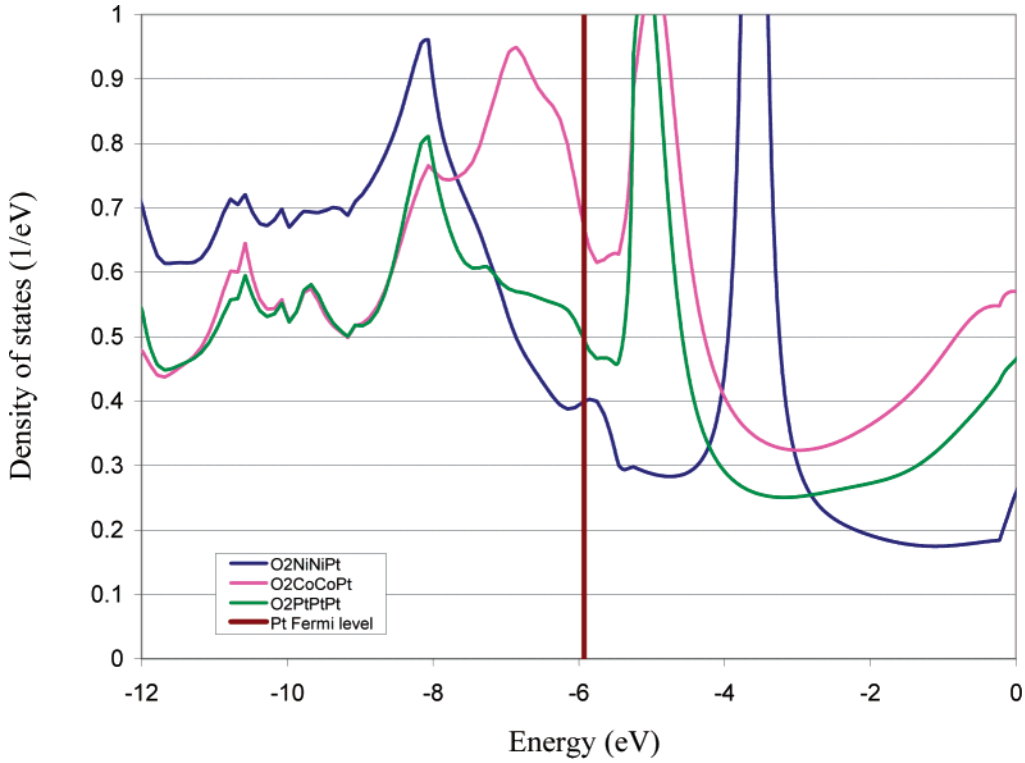

Figure 3. DOS for the O_2NiNiPt, O_2CoCoPt, and O_2PtPtPt, all embedded in a Pt metal. The occupied states of all of the systems are qualitatively similar; however they all differ considerably in the proximity of the Fermi level. Note the decrease in the amount of the available states for O_2NiNiPt (not a good promoter of O_2 dissociation), in contrast with the case of O_2CoCoPt. The first peak corresponding to the unoccupied states for O_2CoCoPt and O_2PtPtPt is located in the same range of energies, but for O_2CoCoPt, the proximity of this peak with the one at the left of the Fermi level is found to be a signal of O_2 dissociation being favored by this system.

the extra Pt atom (not part of the bridge site) seems to help dissociation of O_2 adsorbed on the Co−Co bond, which is evident by comparison with the O_2CoCo case.

Density of States of the Adsorbed O_2 Molecule. Following the Green function approach, we have calculated the density of states of O_2 when the active sites are embedded in the catalyst. Figure 1 illustrates the effect of the metal on the discrete molecular orbitals of O_2. In this case, the optimized O_2Pt_2 system ($m = 3$), with an O−O distance of 1.54 Å and O−Pt distances of 1.93 Å, is subjected to the effect of a Pt background. One important feature is given by the broadening of the peaks corresponding to the energy states of the molecule, which is evident by comparing with the positions of the α and β orbitals corresponding to the O_2 molecule shown as red and blue symbols in the bottom of Figure 1. The energy of the HOMO orbital is −6.54 eV, lying just below the Fermi level of Pt (−5.93 eV), and that of the LUMO orbital is −5.11 eV. In the molecule−metal system, those states are shifted revealing the transfer of electrons from the metal to the antibonding π^* states of O_2. The α DOS is the dominant contribution to the occupied

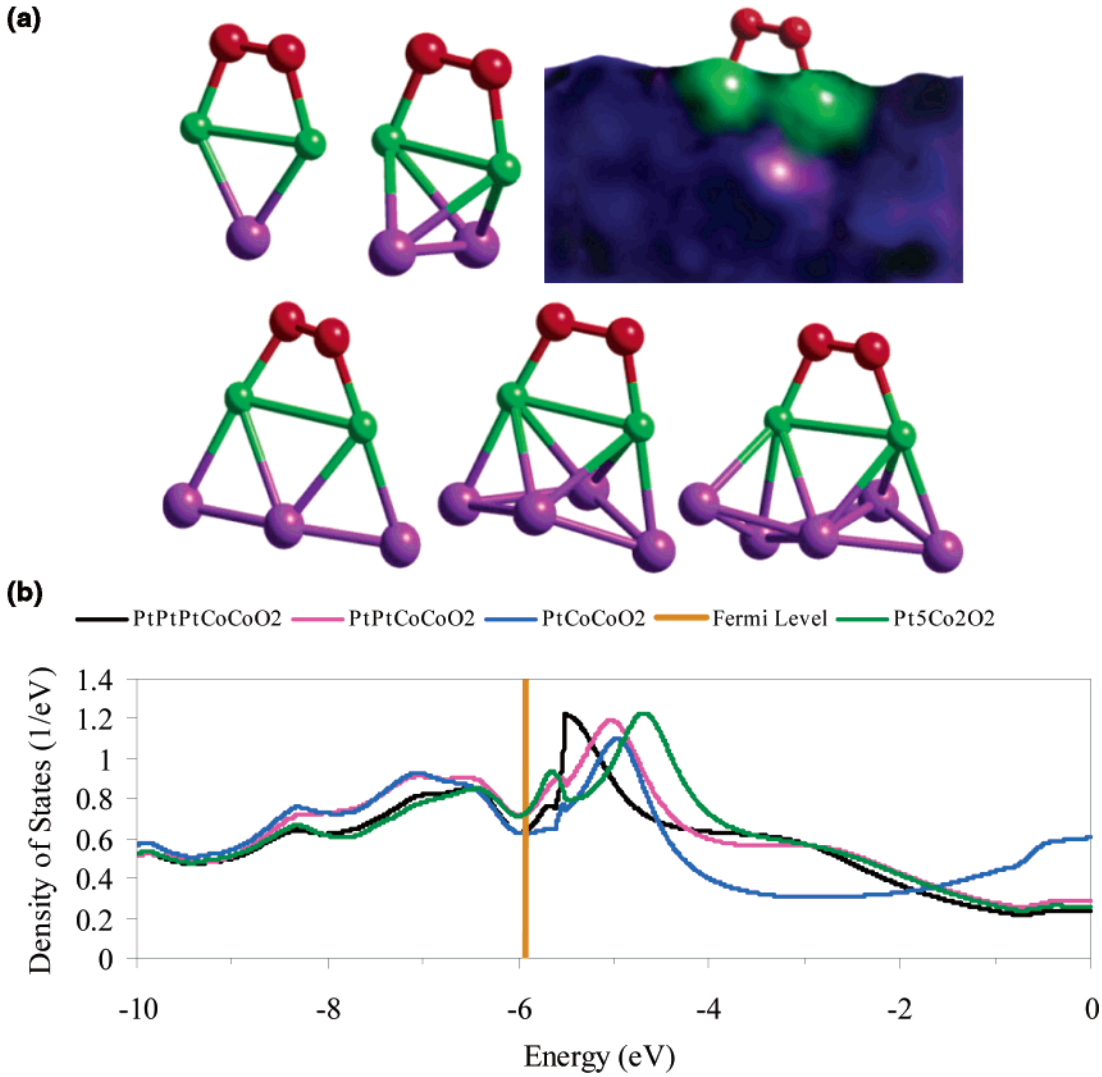

Figure 4. Optimized geometries (a) for oxygen (red), platinum (purple), and cobalt (green) with increasing number of Pt atoms and a pictorial view of the effect of the continuum Pt background and (b) density of states of O_2Co_2Pt (blue), $O_2Co_2Pt_2$ (purple), $O_2Co_2Pt_3$ (black), and $O_2Co_2Pt_5$ (green) with geometries as illustrated in Figure 3a. In all cases, the metal background is Pt.

states, whereas the empty states are defined by the contributions of the β states.

It is crucial to understand how the DOS in the proximity of the Fermi level could provide indications about O_2 dissociation induced by the metal. To analyze this point, we computed the DOS (Figure 2) for an oxygen molecule located parallel to Pt−Pt at 2.1 Å at several O−O bond distances from equilibrium (1.2 Å) to total dissociation (5 Å). The dissociation limit (DOS curves located at the back of the graph) is represented by the atomic orbitals of the oxygen atoms; each is doubly degenerated because there are two atoms. On the other hand, at the O−O distances close to the O−O bond length, the DOS shows that the single peak of O is substituted by two molecular orbitals of the oxygen molecule, usually one above and one below the Fermi level of the metal (Figure 1). The splitting of the single peak becomes clear as the O−O distance decreases, forming the O−O bond. We use this feature, the separation between the peaks corresponding to the frontier molecular orbitals, as an indication of the degree of dissociation of the adsorbed O_2 molecule.

Table 5 displays the values of the DOS for each system evaluated at the Pt Fermi level and the energy difference between the centers of the two peaks located at the left and right of the Fermi level, corresponding to the occupied and unoccupied states of the chemisorbed molecule attached to the metal system. For a metal system to be a good promoter of O_2

TABLE 5: Density of States (DOS) of Each Molecule−Metal System[a]

system	DOS at Pt Fermi level (1/eV)	ΔE between peaks at both sides of Pt Fermi level (eV)	O−O distance at the chemisorbed state (Å)
$O_2PtPtPt$	0.50	3.0	1.41
$O_2PtPtCo$	0.52	4.0	1.38
$O_2PtPtNi$	0.50	4.0	1.38
$O_2PtPtCr$	0.60	3.5	1.37
$O_2PtCoPt$	0.55	2.5	1.45
$O_2PtNiPt$	0.50	3.8	1.40
$O_2PtCrPt$	0.60	1.5	1.47
$O_2PtCoCo$	0.55	3.8	1.40
$O_2PtNiNi$	0.55	3.3	1.41
$O_2PtCrCr$	0.52	3.8	1.41
$O_2CoCoPt$	0.65	2.0	1.49
$O_2NiNiPt$	0.40	4.3	1.38
$O_2CrCrPt$	0.72	1.5	1.41

[a] The metal background is Pt. The difference in energy (ΔE) between the main peak of the occupied states located at the left of the Pt Fermi level and the main peak of the virtual states located at the right of the Pt Fermi level provides an indication of the degree of O_2 dissociation, as shown in Figure 2.

dissociation, we find that the DOS available at the Pt Fermi level should be sufficiently high whereas the ΔE between the main peaks at left and right of the Pt Fermi level should be small enough so that it becomes closer to the undissociated state represented by a single peak located at the Pt Fermi level (Figure 2).

In agreement with the previous discussion, it is observed that the first group of systems, in which O_2 adsorbs on a Pt−Pt bond with both Pt atoms bonded to a foreign metal (Co, Ni, Cr), does not represent an improvement over the pure Pt case. Good degree of dissociation is found when O_2 bonds to a Pt−X metal with both Pt and X bonded to a Pt atom, except when X = Ni. Not much improvement is obtained when O_2 is chemisorbed on a Pt−X site with both Pt and X bonded to an X atom. The best promoter of O_2 dissociation is found to be the case of O_2 adsorbed to a Co−Co bond in which both Co atoms are connected to a Pt atom, and the worst case is O_2 adsorbed to a Ni−Ni bond with both Ni atoms connected to a Pt atom. In all cases, the small system in Table 5 is embedded in a Pt metal background. Figure 3 illustrates these concepts for three systems; one in which the active sites are Pt atoms (O_2PtPtPt) is compared with the "worst" O_2NiNiPt and the "best" O_2CoCoPt cases.

To investigate the effect of extra Pt atoms in the cluster, we further analyzed the $O_2CoCoPt_n$ system with $n = 1$, 2, 3, and 5. In all cases, two Co atoms are directly attached to the O_2 molecule but the number of platinum atoms located at the back of the atoms at the discrete−continuum interface are one, two, three, and five (Figure 4a). The DOS curves are qualitatively very similar but quantitatively different. The differences are stronger on the unoccupied side than in the occupied one (Figure 4b). This is certainly expected in any ab initio procedure; the occupied states are better calculated than the unoccupied states. The separation between the peaks at the left and right of the Fermi level of the metal is relatively small, indicating the proximity to a state where both peaks merge, signaling O_2 dissociation. As the number of Pt atoms connected to the Co atoms increases ($n = 3$ and 5), the development of a second peak very close to the Fermi level of Pt on the side of the unoccupied orbitals becomes more pronounced.

Summary and Conclusions

A new procedure is presented that permits one to investigate the behavior of active catalytic sites including the effect of the bulk environment on the reaction. The procedure is illustrated for O_2 dissociation on bimetallic active sites in which Co, Cr, or Ni atoms are mixed with Pt atoms all embedded in a Pt matrix.

It has been speculated on the basis of experimental results that Ni, Co, and Cr would become oxidized and act as "sacrificial sites" where other species may adsorb, leaving the Pt sites available for O_2 dissociation. Although this may be the case for Ni, we show that alternative mechanisms are possible, especially for Co and Cr, which act as active sites for O_2 dissociation.

Our theoretical analysis permits us to identify the best ensembles of bimetallic active sites that favor O_2 dissociation. It is found that O_2 chemisorption on O_2XPt and O_2XXPt (X = Co and Cr) are the best active sites to promote O_2 dissociation. On the other hand, ensembles involving Ni atoms produce similar degrees of O_2 dissociation as those of pure Pt; thus, other mechanisms, which would enable enhanced activities, may take place as previously suggested.

Acknowledgment. This work is supported by the Department of Energy/Basic Energy Sciences, Grant DE-FG02-1ER15249. The use of computational facilities at the National Energy Research Scientific Computing Center, NERSC, and at the Major Shared Resource Center (ARL MSRC) is gratefully acknowledged.

References and Notes

(1) Adzic, R. In *Recent advances in the kinetics of oxygen reduction* in *Electrocatalysis*; Ross, P. N., Ed.; Wiley-VCH: New York, 1998; pp 197−242.

(2) Luntz, A. C.; Williams, M. D.; Bethune, D. S. The Sticking of O2 on a Pt(111) surface. *J. Chem. Phys.* **1988**, *89*, 4381.

(3) Nolan, P. D.; Lutz, B. R.; Tanaka, P. L.; Davis, J. E.; Mullins, C. B. Molecularly chemisorbed intermediates to oxygen adsorption on Pt-(111): A molecular beam and electron energy-loss spectroscopy study. *J. Chem. Phys.* **1999**, *111*, 3693−3704.

(4) Luntz, A. C.; Grimblot, J.; Fowler, D. E. Sequential precursors in dissociative chemisorption: O_2 on Pt(111). *Phys. Rev. B* **1989**, *39*, 12903−12906.

(5) Damjanovic, A.; Brusic, V. Electrode kinetics of oxygen reduction on oxide-free platinum electrodes. *Electrochim. Acta* **1967**, *12*, 615−628.

(6) Markovic, N. M.; Ross, P. N. Electrocatalysis at well-defined surfaces: Kinetics of oxygen reduction and hydrogen oxidation/evolution on Pt(*hkl*) electrodes. In *Interfacial Electrochemistry. Theory, Experiment and Applications*; Wieckowski, A., Ed.; Marcel Dekker: New York, 1999; pp 821−841.

(7) Markovic, N. M.; Ross, P. N. Surface Science Studies of Model Fuel Cells Electrocatalysts. *Surf. Sci. Rep.* **2002**, *286*, 1−113.

(8) Sheppard, S. A.; Campbell, S. A.; Smith, J. R.; Lloyd, G. W.; Ralph, T. R.; Walsh, F. C. Electrochemical and microscopic characterization of platinum-coated perfluorosulfonic acid (Nafion 117) materials. *Analyst* **1998**, *123*, 1923−1929.

(9) Markovic, N. M.; Ross, P. N. Electrocatalysts by design: from the tailored surface to a commercial catalyst. *Electrochim. Acta* **2000**, *45*, 4101−4115.

(10) Drillet, J. F.; Ee, A.; Friedemann, J.; Kotz, R.; Schnyder, B.; Schmidt, V. M. Oxygen reduction at Pt and Pt70Ni30 in H2SO4/CH3OH solution. *Electrochim. Acta* **2002**, *47*, 1983−1988.

(11) Toda, T.; Igarashi, H.; Watanabe, M. Enhancement of the electrocatalytic O_2 reduction on Pt−Fe alloys. *J. Electroanal. Chem.* **1999**, *460*, 258−262.

(12) Mukerjee, S.; Srinivasan, S. Enhanced electrocatalysis of oxygen reduction on platinum alloys in proton-exchange membrane fuel cells. *J. Electroanal. Chem.* **1993**, *357*, 201−224.

(13) Mukerjee, S.; Srinivasan, S.; Soriaga, M. P. Effect of Preparation Conditions of Pt Alloys on Their Electronic, Structural, and Electrocatalytic Activities for Oxygen Reduction−XRD, XAS, and Electrochemical Studies. *J. Phys. Chem.* **1995**, *99*, 4577−4589.

(14) Stamenkovic, V.; Schmidt, T. J.; Ross, P. N.; Markovic, N. M. Surface Composition Effects in Electrocatalysis: Kinetics of Oxygen Reduction on Well-Defined Pt_3Ni and Pt_3Co Alloy Surfaces. *J. Phys. Chem. B* **2002**, *106*, 11970−11979.

(15) Becke, A. D. Density-functional thermochemistry III. The role of exact exchange. *J. Chem. Phys.* **1993**, *98*, 5648−5652.

(16) Perdew, J. P.; Chevary, J. A.; Vosko, S. H.; Jackson, K. A.; Pederson, M. R.; Singh, D. J.; Fiolhais, C. Atoms, Molecules, Solids, and Surfaces: Applications of the Generalized Gradient Approximation for Exchange and Correlation. *Phys. Rev. B* **1992**, *46*, 6671−6687.

(17) Perdew, J. P.; Wang, Y. Accurate and Simple Analytic Representation of the Electron-Gas Correlation Energy. *Phys. Rev. B* **1992**, *45*, 13244−13249.

(18) Wadt, W. R.; Hay, P. J. Ab initio effective core potentials for molecular calculations. Potentials for main group elements Na to Bi. *J. Chem. Phys.* **1985**, *82*, 284−298.

(19) Hay, P. J.; Wadt, W. R. Ab initio effective core potentials for molecular calculations. Potentials for the transition metal atoms Sc to Hg. *J. Chem. Phys.* **1985**, *82*, 270−283.

(20) Hay, P. J.; Wadt, W. R. Ab initio effective core potentials for molecular calculations. Potentials for K to Au including the outermost core orbitals. *J. Chem. Phys.* **1985**, *82*, 299−310.

(21) Frisch, M. J.; Trucks, G. W.; Schlegel, H. B.; Scuseria, G. E.; Robb, M. A.; Cheeseman, J. R.; Zakrzewski, V. G.; Montgomery, J. A., Jr.; Stratmann, R. E.; Burant, J. C.; Dapprich, S.; Millam, J. M.; Daniels, A. D.; Kudin, K. N.; Strain, M. C.; Farkas, O.; Tomasi, J.; Barone, V.; Cossi, M.; Cammi, R.; Mennucci, B.; Pomelli, C.; Adamo, C.; Clifford, S.; Ochterski, J.; Petersson, G. A.; Ayala, P. Y.; Cui, Q.; Morokuma, K.; Malick, D. K.; Rabuck, A. D.; Raghavachari, K.; Foresman, J. B.; Cioslowski, J.; Ortiz, J. V.; Stefanov, B. B.; Liu, G.; Liashenko, A.; Piskorz, P.; Komaromi, I.; Gomperts, R.; Martin, R. L.; Fox, D. J.; Keith, T.; Al-Laham, M. A.; Peng, C. Y.; Nanayakkara, A.; Gonzalez, C.; Challacombe, M.; Gill, P. M. W.; Johnson, B. G.; Chen, W.; Wong, M. W.; Andres, J. L.; Head-Gordon, M.; Replogle, E. S.; Pople, J. A. *Gaussian 98*, revision A.11; Gaussian, Inc.: Pittsburgh, PA, 1998.

(22) Seminario, J. M.; Zacarias, A. G.; Tour, J. M. Molecular Alligator Clips for Single Molecule Electronics. Studies of Group 16 and Isonitriles Interfaced with Au Contacts. *J. Am. Chem. Soc.* **1999**, *121*, 411−416.

(23) Mainardi, D. S.; Balbuena, P. B. Hydrogen and Oxygen Adsorption on Rh_n ($n = 1-6$) Clusters. *J. Phys. Chem. A*, in press.

(24) Seminario, J. M.; Zacarias, A. G.; Derosa, P. A. Theoretical Analysis of Complementary Molecular Memory Devices. *J. Phys. Chem. A* **2001**, *105*, 791−795.

(25) Derosa, P. A.; Seminario, J. M. Electron Transport through Single Molecules: Scattering Treatment Using Density Functional and Green Function Theories. *J. Phys. Chem. B* **2001**, *105*, 471−481.

(26) Balbuena, P. B.; Derosa, P. A.; Seminario, J. M. Density Functional Theory Study of Copper Clusters. *J. Phys. Chem. B* **1999**, *103*, 2830−2840.

(27) (a) Mulliken, R. S. Electronic Population Analysis on LCAO-MO Molecular Wave Functions. *J. Chem. Phys.* **1955**, *23*, 1833. (b) Mulliken, R. S. *J. Chem. Phys.* **1955**, *23*, 1841. (c) Mulliken, R. S. *J. Chem. Phys.* **1955**, 2338. (d) Mulliken, R. S. *J. Chem. Phys.* **1955**, 2343.

(28) Parr, R. G.; Yang, W. *Density Functional Theory of Atoms and Molecules*; Oxford University Press: Oxford, U.K., 1989.

(29) Seminario, J. M., Politzer, P., Eds., *Modern Density Functional Theory: A Tool for Chemistry*; Elsevier: Amsterdam, 1995.

(30) Roetti, C. The CRYSTAL Code. In *Lecture Notes in Chemistry*; Pisani, C. Springer-Verlag: Berlin, Heidelberg, 1996; pp 125−137.

(31) Towler, M. D.; Zupan, A.; Causa, M. Density functional theory in periodic systems using local Gaussian basis sets. *Comput. Phys. Commun.* **1996**, *98*, 181−205.

(32) Roetti, C. The Crystal Code. In *Quantum-Mechanical Ab-initio Calculation of the Properties of Crystalline Materials*; Pisani, C., Ed.; Springer: Berlin, 1996.

(33) Cundari, T. R.; Stevens, W. J. Effective Core Potential Methods for the Lanthanides. *J. Chem. Phys.* **1993**, *98*, 5555−5565.

(34) Stevens, W. J.; Krauss, M.; Basch, H.; Jasien, P. G. Relativistic Compact Effective Potentials and Efficient, Shared-Exponent Basis-Sets for the 3rd-Row: 4th-Row: and 5th-Row Atoms. *Can. J. Chem.* **1992**, *70*, 612−630.

(35) Seminario, J. M.; Derosa, P. A. Molecular Gain in a Thiotolane System. *J. Am. Chem. Soc.* **2001**, *123*, 12418−12419.

(36) Seminario, J. M.; Zacarias, A. G.; Derosa, P. A. Analysis of a Dinitro-Based Molecular Device. *J. Chem. Phys.* **2002**, *116*, 1671−1683.

(37) Derosa, P. A.; Zacarias, A. C.; Seminario, J. M. Application of Density Functional Theory to the Study and Design of Molecular Electronic Devices: The Metal-Molecule Interface. In *Reviews of Modern Quantum Chemistry*; Sen, K. D., Ed.; World Scientific: Singapore, 2002; pp 1537−1567.

(38) Seminario, J. M.; De La Cruz, C. E.; Derosa, P. A. A Theoretical Analysis of Metal−Molecule Contacts. *J. Am. Chem. Soc.* **2001**, *123*, 5616−5617.

(39) Seminario, J. M.; Zacarias, A. G.; Derosa, P. A. Analysis of a dinitro-based molecular device. *J. Chem. Phys.* **2002**, *116*, 1671−1683.

(40) Gland, J. L. Molecular and atomic adsorption of oxygen on the Pt (111) and Pt (S)-12 (111) x (111) surfaces. *Surf. Sci.* **1980**, *93*, 487−514.

(41) Gland, J. L.; Sexton, B. A.; Fisher, G. B. Oxygen interactions with the Pt (111) surface. *Surf. Sci.* **1980**, *95*, 587−602.

(42) Li, T.; Balbuena, P. B. Computational Studies of the Interactions of Oxygen with Platinum Clusters. *J. Phys. Chem. B* **2001**, *105*, 9943−9952.

(43) Li, T.; Balbuena, P. B. Oxygen Reduction on a Platinum Surface: A Cluster Model Study. *Chem. Phys. Lett.* **2003**, *367*, 439−447.

(44) Eichler, A.; Hafner, J. Molecular Precursors in the dissociative adsorption of O_2 on Pt (111). *Phys. Rev. Lett.* **1997**, *79*, 4481−4484.

(45) Eichler, A.; Mittendorfer, F.; Hafner, J. Precursor-mediated adsorption of oxygen on the (111) surfaces of platinum-group metals. *Phys. Rev. B* **2000**, *62*, 4744−4755.